Sensors and Actuators Reports 6 (2023) 100173

Contents lists available at ScienceDirect

Sensors and Actuators Reports

journal homepage: www.sciencedirect.com/journal/sensors-and-actuators-reports

Plasmonic microcarriers for sensing and cell expansion

Charlotte B.A. Stoffels [a,b], Patrick Grysan [a], Caroline Sion [e], Rishabh Rastogi [a,c], Matteo Beggiato [a,d], Eric Olmos [e,*], Sivashankar Krishnamoorthy [a,*]

[a] Materials Research and Technology (MRT), Luxembourg Institute of Science and Technology (LIST), 41, Rue du Brill, Belvaux L-4422, Luxembourg
[b] Department of Chemical and Materials Engineering, University of Liège, B6a, Quartier Agora, 11, Allée du six Août, Liège B-4000, Belgium
[c] Laboratory Light, nanomaterials & nanotechnologies – L2n, the University of Technology of Troyes & CNRS ERL 7004, 12 rue Marie Curie, Troyes 10000, France
[d] Doctoral School in Science and Engineering (DSSE), Faculty of Science, Technology and Medicine (FSTM), University of Luxembourg, Belval, Luxembourg
[e] Université de Lorraine, CNRS, LRGP, F-54001 Nancy, France

ARTICLE INFO

Keywords:
Microcarrier
Plasmonics
Nanoparticles
Biosensor
Hydrogel
Cell culture
Gold nanoparticle
Self-assembly

ABSTRACT

Microcarriers (MCs, typically 50–200 μm) are promising growth supports for high-throughput cell expansion, with capability to overcome the limitations of surface area availability and nutrient access encountered by cell culture in 2D well plate configurations. Equipping MCs with in-built capability to sense molecular biomarkers is a key step forward to meet the emerging demands of personalized cell-based therapies. However, integrating sensing functionality into MCs is non-trivial due to fabrication limitations imposed by their large size, curved surfaces, and their suspension in fluid. If achieved, the sensor-integrated MCs should face further concerns of reduced stability and cytocompatibility during cell-culture. Here we demonstrate plasmonic microcarriers (PMCs) that integrate spectroscopic sensing and cell expansion functions through the deposition of gold nanoparticle (AuNP) assemblies on dextran-based MCs. Hydrogel characteristics of the dextran microcarriers was found to profoundly enhance the binding density and kinetics of AuNPs, as seen by attainment of saturated densities in few seconds, and at nanoparticle concentrations only twice that of the surface sites. The approaches to prepare PMCs are distinguished by simple, scalable routes, without need for sophisticated lab infrastructure. The capability of PMCs to act as spectroscopic transducers was demonstrated by surface-enhanced spectroscopic (SERS) detection of a model molecular probe. The growth, proliferation and migration of human mesenchymal stem cells on the PMCs was found to be comparable to that of the uncoated MCs. The results pave the way to smart, multifunctional cell growth supports to interrogate, control and report cell behavior during culture.

1. Introduction

Sensors that enable detection of molecular biomarkers are of high interest for diagnosis and therapy including companion diagnostics [1], single-cell devices [2], in vitro models and implant devices [3]. Nanoscale sensors are promising as they deliver high sensitivity and quick response times within miniaturized footprints. Such sensors can also help to monitor cell viability and behavior during culture, thus enabling the optimization of parameters and enables quality assurance during cell culture [4–6].Cell culture markets focus on harvesting stem cells for cell-based therapies to cater to numerous health ailments. Cell expansion has traditionally been performed using cell-culture on 2D substrates, while recent advances have emphasized microcarriers as a promising alternative, as they are better adapted to large-scale production of stem cells, such as mesenchymal stem cells [7–9]. Microcarriers (MCs) have dimensions in the order of 50–200 μm and enable cell expansion of anchorage-dependent cells, with advantages of better nutrient availability, enhanced surface areas, and automated and high-throughput harvesting of cells within the controlled environment of bioreactors. MCs made of organic as well as inorganic materials, presenting different surface chemistries are commercially available.

Newer MCs with engineered surface and bulk properties are however sought to meet the emerging demands of stem cell expansion, and their induction to different lineages towards cell-based regenerative therapies. Efforts to engineer MCs have been aimed at controlling topographic or chemical cues to influence cell-growth and differentiation, preserving stemness of stem cells, promoting stem cell differentiation into the desired cell-type and enabling an easy release of attached cells to enable reuse of MCs. Beyond these cell-instructive goals, a significant advancement would be to introduce sensing functions that can help

* Corresponding authors.
E-mail addresses: eric.olmos@univ-lorraine.fr (E. Olmos), sivashankar.krishnamoorthy@list.lu (S. Krishnamoorthy).

https://doi.org/10.1016/j.snr.2023.100173
Received 11 June 2023; Received in revised form 23 August 2023; Accepted 25 August 2023
Available online 26 August 2023

monitor cell-health during cell-culture and to report biomarkers of interest. Biomarkers to transduce signaling molecules involved in cell-cell interactions, cell differentiation, and proliferation, and secretory proteins have been of high significance for applications in cell-based therapies, immunology, vaccine, in vitro models and biomanufacturing [10–14]. However, integrating sensing functions on a microcarrier introduces multiple concerns, including (a) changes to bio-interface properties that may adversely impact cytocompatibility, (b) loss of the stability and sensitivity of the sensor within cell-culture media and (c) limited routes to fabricate on a large 3D object that is suspended in a medium, as compared to fabrication on a planar substrate.

Currently, no earlier work in the literature have shown microcarriers capable of supporting cell culture as well as molecular sensing functions. On the other hand, a large body of literature exists on much smaller microbeads that are optically encoded, or tagged with receptors for biomarkers, for targeted use within bead-based assays in biomedical diagnostics applications [15–17]. These microbeads are few microns wide, and thus are 2 orders of magnitude smaller than the typical microcarriers used for cell culture. Extrapolating the processes designed for small micron sized beads to large, sub-millimeter scale microcarriers is not straight-forward due to the need to factor in the significant increase in surface areas (by 3–6 orders of magnitude per sphere) that reduces the ability to integrate sensing layers and could also reduce sensing performance (due to reduced analyte capture by the beads).

Here, we demonstrate microcarriers with integrated plasmonic sensing capabilities, by attaching high density of gold nanoparticles (AuNPs) onto the surface of dextran-based hydrogel microcarriers. Gold, especially, is well suited as the material of choice, given its biocompatibility, stability in cell-culture media, and the unique optical properties that can be exploited to transduce biochemical events using plasmonic detection schemes. Exploiting the optical properties of AuNPs to transduce biochemical information using plasmon-enhanced spectroscopies (PES) such as surface-enhanced Raman or metal-enhanced fluorescence are of high interest, given their ability to pick up analyte's spectral signatures with high sensitivity within few seconds. However, achieving high signal enhancements in PES requires closely separated nanoparticles to maximize enhancement of electromagnetic fields [18–20]. Microcarriers covered with uniform, high density assemblies of nanoparticles have not been demonstrated before.

Different routes to fabricate gold nanoparticle assemblies has been reported in literature, including electrostatic self-assembly (ESA), [19,21,22] self-assembled monolayers with thiol end groups [23], hydrophobic interactions [24], galvanic displacement [25], solution-phase deposition processes [26], and surface-dewetting [27]. Amongst these, ESA stands out due to the ease of attaining uniform, conformal coverage of stable nanoparticle monolayers on different material surfaces [19,21,22]. However, the surface coverage by ESA is theoretically limited to 54.7% based on the random sequential adsorption models (RSA) [28]. The empirically attained surface coverages reported in the literature are still lower, typically amounting to fifth of these limits (~10–15%) [29–31]. The low surface coverages typically result from lack of optimal conditions for ESA including nanoparticle concentrations, inadequate exposure durations and the choice of underlying surface functionalization. The surface coverage can be increased by other means, including attachment to topographically patterned surfaces [32–34], encapsulation within 3D matrices [35,36], and preparing colloidal multilayers [37,38]. Extending ESA to a large object as the MCs pose concerns of ensuring uniformity and high-density of coverage, within practical time frames. In this direction, we demonstrate how the hydrogel characteristics of the dextran-based MCs can enable quick, conformal attachment of AuNPs at high densities. The optical/spectroscopic characteristics of the PMCs were found to be well suited for molecular detection by surface-enhanced Raman spectroscopy. Detailed understanding of the internal/external structure of the PMCs helps realizing geometric models that can be used to understand formation of AuNP assembly on MCs, optical/spectroscopic response of the PMCs, and the cell-PMC interactions. The performance of the plasmonic MCs to support growth and migration of human mesenchymal stem cells is demonstrated through different cell biology tests. The results pave the way to novel microcarriers that can simultaneously support cell expansion as well as sensing of molecular biomarkers. The approaches carry broader applicability to the design and engineering of range of other 3D nano-bio interfaces.

2. Experimental

2.1. Materials

Trisodium citrate ($Na_3C_6H_5O_7$), hydrogen tetrachloroaurate(III) trihydrate ($HAuCl_4{\cdot}3H_2O$) ($\geq$ 99.9%), cytodex-1, 1-naphthalenethiol (NT), n-hexane as an anhydrous solvent with 99% purity were purchased from Sigma-Aldrich. AFM tips were purchased from NanoAndMore. MilliQ water (18.2 MΩcm, Millipore) was used for the preparation of the solutions and all rinses. Alpha-minimum essential medium (α-MEM medium) was purchased from Lonza Biosciences (BE12–169F). 5% of Human Platelet Lysate (HPL) was purchased from Cook Regentec (PL-NH-500). Glutamine (Sigma G7513), and antibiotic antimycotic solution (A5955) were purchased from Sigma-Aldrich.

2.2. AuNP coating of microcarriers

Citrate stabilized gold nanoparticle suspension (pH 6) was synthesized following the Turkevich method, by reducing gold chloride trihydrate solution (1 mM) by sodium citrate dihydrate (38.8 M) under boiling conditions to obtain nanoparticle of the desired diameter [39–41]. A fixed quantity of Cytodex-1 (MCs) was dispersed and incubated in aqueous solutions containing different concentrations of AuNPs for durations of 3 h (Table S1). The microcarriers were subsequently washed with water by pelleting and re-suspending in milli-Q water, to remove unbound or loosely bound Au nanoparticles by centrifuging at 1300 g for 2 min.

2.3. Dynamic light scattering (DLS)

DLS was used to determine the hydrodynamic size and zeta potential of the AuNP suspension using Zetasizer Nano ZS (Malvern Panalytical). Disposable folded capillary zeta cell (Malvern Panalytical) was used for the measurement of both parameters.

2.4. Ultramicrotomy

Au nanoparticle covered microcarriers were sliced into segments of a predefined depth using ultra-microtomy, to check for AuNP distribution inside the microcarriers. The water floating technique commonly usually used to recover the microtomed slices did not work as the slice of DEAE-Dextran completely disintegrated in the water. Liquid propane or dried recovery was mandatory.

2.5. Optical microscopy

Images of the microcarriers were acquired using Olympus Microscope BX51 under 10x and 50x magnification, using an Olympus Stream image analysis software. The sample for observation was prepared by sandwiching a few drops of microcarrier suspension between two glass wafers. The results were acquired and analyzed using Ocean View and OriginLab software, respectively. Optical spectra in the visible wavelength range of the AuNPs and AuNP@MCs were obtained using TECAN Infinite M1000 PRO plate reader.

2.6. Scanning electron microscopy (SEM)

SEM micrographs of the microcarriers were obtained using Helios

NanoLab™ 650 microscope operating at an accelerating voltage of 1 – 3 kV (for MCs and AuNP@MCs) or 20 kV (AuNPs) and a working distance between 4 – 6 mm. The sample was prepared by drying 2 μL of MCs directly on a clean conductive substrate at room temperature.

2.7. Atomic force microscopy (AFM)

Topography measurements of the MCs before and after adsorption of AuNPs were performed using AFM under dry conditions, using Innova system (Bruker, USA). Measurements were performed in tapping mode using a silicon AFM probe OPUS 160AC NA (Mikromasch, Bulgaria) with a force constant of 26 N.m^{-1} and a resonance frequency of 300 kHz.

2.8. Raman spectroscopy

Plasmonic MCs (AuNP@MCs) were functionalized with 1-napthalene thiol (NT) (used as a molecular probe) in ethanol overnight. After incubation, the AuNP@MCs were washed 5 times with absolute ethanol to remove excess and any loosely bound NT. Raman spectra were recorded in the [100–4000] cm^{-1} range using Renishaw inVia™ Raman microscope equipped with a high-powered near-IR laser diode working at 785 nm and a visible laser diode working at 633 nm. Before spectra acquisition, an optical microscope (Olympus; objective, x50L) was used to focus the laser beam. The laser power of 0.9 *mW* was used for excitation. For each spectrum, 6 accumulations of 5 s were recorded. To ensure representative characterization of surfaces, multiple measurements were recorded on different areas of a chosen microcarrier as well as from different microcarriers. Results were analyzed using WiRE™ and OriginLab software. Spectra acquired were smoothed, normalized. Wet measurements were acquired after adding a droplet of water onto the dry MCs on glass slide.

2.9. MSC isolation and culture under static conditions

Umbilical cord stem cells were extracted from fresh umbilical cords of babies just born (CHU Nancy). Umbilical cords were treated during 24 h following birth. The method of extraction was non-enzymatic using cells spontaneous migration on the 175 cm^2 plastic culture flask. The cell culture medium was alpha-minimum essential medium (α-MEM medium) supplemented with 5% of Human Platelet Lysate (HPL), 4 mM glutamine, and 1% antibiotics (Antibiotic antimycotic solution). The medium was changed twice a week. After ten days, the remaining adherent cells were trypsinized and seeded in new 175 cm^2 T-flasks at a density of 3 000 cells cm^{-2}. After one supplementary passage, WJ-MSC was pooled and cryopreserved at a concentration of 2 x 10^6 cells mL^{-1}, in human platelet lysate and 10% of dimethyl sulfoxide (DMSO) for cell banking and kept in liquid nitrogen. Thereafter, cells were thawed and seeded at a concentration of 3000 cells cm^{-2} in T-175 cm^2 and cultivated for a week before their use in dynamic conditions.

2.10. Biocompatibility and cell migration tests

Different biocompatibility tests were performed to compare MCs and AuNP@MCs, viz., cell growth assays, autoclaving assays (effect of autoclaving) and bead-to-bead migration assays (to test migration of cells cultured on MCs to freshly added AuNP@MCs). 590 μl of MCs or AuNP@MCs suspensions (20 g/l) and 5 ml of cell culture medium was added into the 6 well-plates low bindings (Costar 6 well-plate ultra-low attachment Corning 3471). MCs were kept in that container for 1 h at 37 °C and 5% CO_2. Cells were detached at passage 5 and harvested from their container flasks by trypsinization (TrypLE Gibco 12,604,013). They were added into the 6-well plates already containing the microcarriers at a concentration of 80,000 cells/ml. The cell density was thus about 7500 cells/cm^2. Cells and microcarriers were incubated in the cell culture medium to allow adhesion of the cells on the microcarriers. After 1 h, cells anchored on microcarriers were put in agitation at 70 rpm (37 °C; 5% CO_2). A sample of the cell culture medium was withdrawn on a daily basis to measure glucose and glutamine consumption, as well as lactate, ammonium production, and lactate dehydrogenase release. Cell viability was assessed by fluorescence microscopy. Cells were mixed with DAPI, Calcein AM and Ethidium Homodimer-1 (EthD-1) molecules to stain cells, live cells, and dead cells, respectively. On day 4, 50% of the cell culture medium was renewed. For the migration assay (co-culture), AuNP@MCs were added to the culture plate with MCs on day 4. After 1 h of incubation, the agitation could be restarted (70 RPM).

3. Results and discussion

3.1. Fabrication of plasmonic microcarriers

Plasmonic microcarriers were prepared by electrostatic attachment of AuNPs onto MCs containing diethylaminoethyl (DEAE) groups (DEAE-dextran) (Fig. 1). The DEAE-dextran MCs were shown in earlier literature to carry promising attributes for use as support for culture of adherent cells and commercially available under the name of Cytodex®. Due to the basicity of the constituent secondary amino groups of DEAE, these MCs exhibit positive charge at neutral and acidic pH. The positive charge allows the MC to attract negatively charged citrate stabilized gold nanoparticles with a diameter of 11.6 ± 0.79 nm, exhibiting a zeta potential of −34 mV at pH 6 (Fig. 1). The MCs were exposed to AuNP suspensions of systematically increasing concentrations, to identify conditions for saturated the surface coverage of AuNPs (Table S1). The SEM shows a saturated coverage of AuNPs to be attained at a suspension concentration of nanoparticles approximately twice that of available surface sites. MCs exposed to AuNPs at lower concentrations showed a patchy, yet homogeneous coverage (Fig. S1, Fig. S2). By virtue of being a cross-linked hydrogel, the MC experiences heavy swelling in an aqueous medium. However, the degree of swelling was found to reduce from 260% to 141%, upon saturated coverage of gold nanoparticles (Fig. 2).

The degree of swelling was calculated as in Eq. (1), where D_{aq} and D_{dry} indicate the diameters of the microcarriers (MC or AuNP@MC) in aqueous or dry states, respectively. The size of the AuNP@MC (dry) was taken to be the same as MC (dry) based on the thickness of AuNP layer around the MCs (images of microtomy slices, Fig. 3b), and based on the SEM images for the dry AuNP@MC (Fig. 3a).

$$\%\ swelling = \frac{D_{aq} - D_{dry}}{D_{dry}} \times 100 \quad (1)$$

The reduced swelling of the AuNP@MCs may be attributed to the AuNP binding to multiple polymeric chains, resulting in the crosslinking the surface of the MCs. The MCs were analyzed further to check for the presence of AuNPs in the bulk. To perform this, AuNP@MCs were pelleted from suspension, then air-dried and sectioned by ultramicrotomy, and analyzed by SEM and NanoSIMS. Drying resulted in the partial fusion of the microcarrier interfaces, as observed in Fig. 3a. The investigation of the sections reveals the presence of nanoparticles to be restricted to the surface of the microcarriers and absent within the MC. Further NanoSIMS, measuring the elemental distribution of Au on the microtome slice confirm the observation from SEM (Fig. 3). Comparison of AFM images of uncoated MCs and MCs coated with saturated coverage of AuNPs reveal an increase in rms roughness from 23 nm to 39 nm (Fig. S3).

Based on internal/external structural analysis by optical microscopy, SEM, AFM and NanoSIMS, the AuNP@MC can be represented by a simple geometric model, with AuNP evenly distributed in the exterior of the swollen MC (Fig. 4). The attachment of AuNPs to the MC is treated under random sequential adsorption models (RSA) with expected maximum coverage (or jamming limit) at 54.7%. The number of particles necessary for saturated surface coverage is derived from the surface area of the microcarriers in the AuNP suspension (S_{MC}) and the 2D footprint of the gold nanoparticles (S_{NP}) as in Eq. (2). The values for S_{MC}

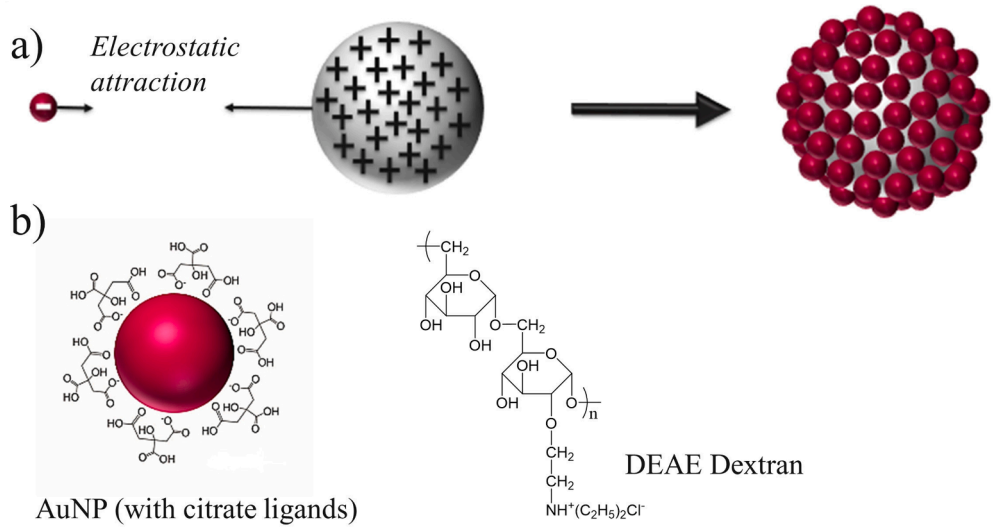

Fig. 1. (a) Schematic illustration of the formation of PMCs by electrostatic self-assembly of negatively charged AuNPs onto positively charged DEAE-Dextran MCs (b) Illustration of the citrate stabilization on the gold nanoparticles and the molecular structure of DEAE-Dextran that provides the basis for the respective negative and positive charges.

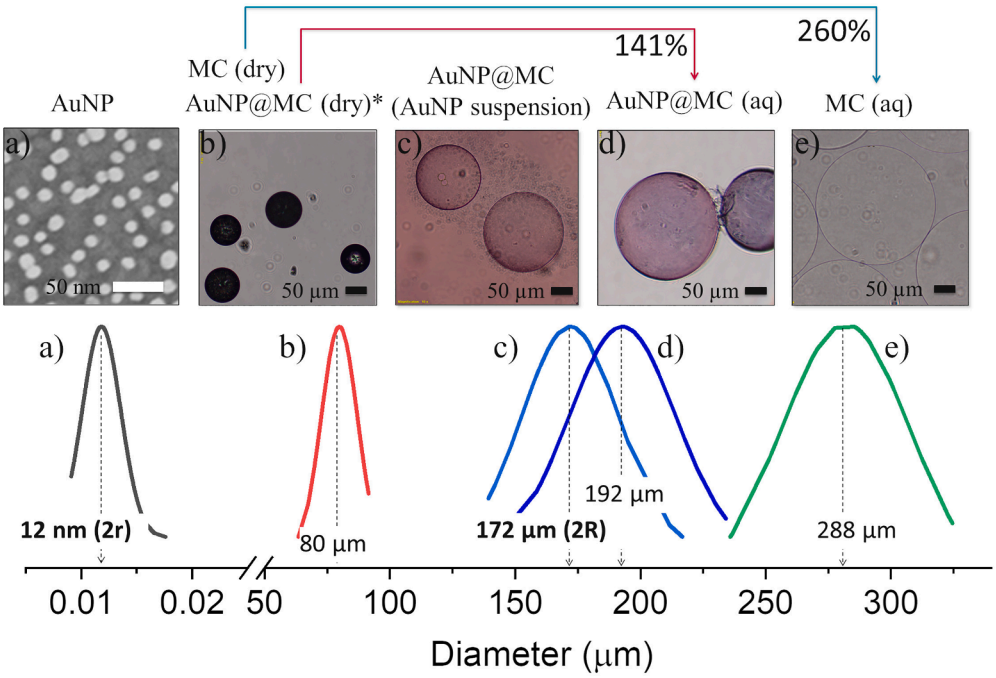

Fig. 2. Comparison of the dimensions of uncoated and coated MCs and the AuNPs used for coating. Size distributions of (a) gold nanoparticles (b) MCs in the dry form (c) AuNP@MCs in AuNP suspension, (d) AuNP@MCs in aqueous medium, (e) MCs in an aqueous medium, (b-e) shown along with their (a) SEM or (b-e) optical micrographs. *AuNP@MC (dry) (image/histograms not shown) is taken to have equivalent dimensions as the MC(dry) to illustrate the decrease in swelling ratios of AuNP@MCs in comparison to MCs. Swelling ratios from MCs and AuNP@MCs are indicated.

and S_{NP} were derived from the mean values of size distribution curves for radii of MC (R) and AuNP (r), determined from optical microscopy and SEM respectively (Fig. 2). This yields the estimate of 4.5×10^8 AuNPs per MC ($[AuNP]_{ideal}$) as expectation for the AuNP surface concentrations at saturated surface coverage.

$$[AuNP]_{ideal} = \frac{54.7\% * S_{MC}}{S_{NP}} = \frac{54.7\% * 4\pi R^2}{\pi r^2} = 2.2\left(\frac{R}{r}\right)^2 \quad (2)$$

3.2. AuNP binding efficiency and optical response of plasmonic microcarriers

The formation of AuNP@MCs was investigated by their optical response when systematically increasing the AuNP solution concentrations per MC ($[AuNP]_{solution}$) by upto 5 times the equivalent AuNP surface concentrations at saturated coverages ($[AuNP]_{ideal}$, Eq. (2)). The number of AuNPs in solution available per microcarrier ($[AuNP]_{solution}$) is calculated by dividing the total number of AuNPs in solution by the total number of microcarriers present in the same volume (Table S1). The total number of AuNPs in the suspension can be estimated from the ratio of the total mass of gold in solution divided by the mass of a AuNP. The mass of gold in solution is known from the molar concentrations of gold salt used during synthesis, all of which is assumed to be reduced to gold. The mass per AuNP is obtained by approximating the AuNP as a sphere with the diameter corresponding to the peak size distribution plots (Fig. 3), thus deriving volume and mass per particle (assuming the density of gold to be the same as bulk gold i.e. 19.32 g/cm^3). The number of MCs per unit volume was obtained from the manufacturer's specification of the number of MCs per gram of dry weight, which amounts to 6.8×10^6 MCs/g for Cytodex-1 [42]. Consequently, the

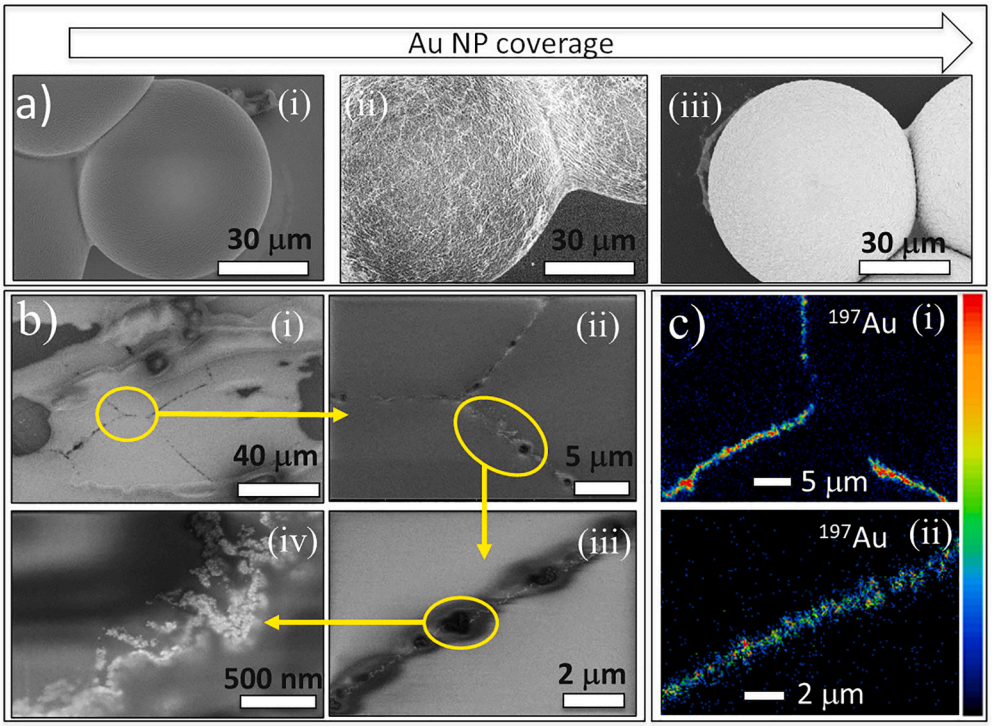

Fig. 3. AuNP distribution on the MC surface. (a,b) Scanning electron microscopy images of (a) MC with increasing concentration of AuNP coverage. (b) Microtomed slices of MCs coated at saturated coverage of nanoparticles focused at the interface between fused microcarriers, with increasing magnifications from i-iv. (c) NanoSIMS maps of ^{197}Au in (c, i) and (c, ii) correspond to the SEM images in (b, i) and (bottom) (b, ii) respectively. (Refer to Fig. S4, Fig. S5 for further microtomy and characterization of microtomed slices).

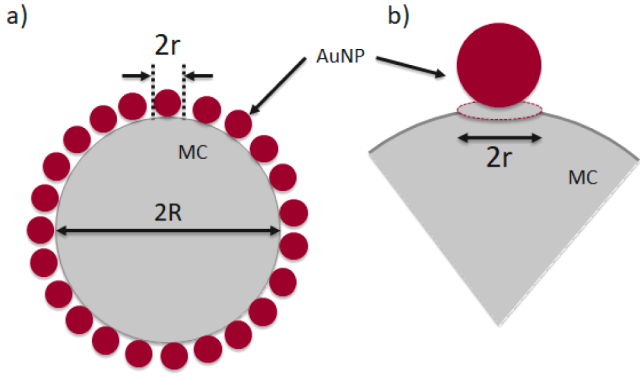

Fig. 4. Geometric model of the AuNP@MC. (a) Schematic illustration of the cross-section of AuNPs attached to the exterior surface of the swollen MC. The radii of the MC and AuNP are shown as R and r respectively (b) Zoomed in illustration of the footprint of the nanoparticle on MC surface. Drawings are not to scale.

number of microcarriers (N_{MCs}) present in a given mass of Cytodex-1 powder (M_{MCs}) is estimated.

AuNP@MCs are easily distinguished from uncoated MCs by optical microscopy (Fig. 5a, Video S1 in Supporting Info). The uncoated MCs are nearly transparent in water, while AuNP@MCs appear purple with an intensity that increases with nanoparticle coverage. The nanoparticle coverage on MCs could be followed by monitoring the absorbance spectra of the aqueous suspension of AuNP@MCs, which shows a systematic increase in the peak wavelength and intensity of the localized surface plasmon resonance (LSPR) peak of AuNPs as a function of increasing surface coverage on the MCs (Fig. 5, Fig. 6a). The increase in peak intensity is also associated with a red-shift of the peak wavelength, in line with expectations for increased plasmonic coupling between adjacent particles due to increased proximity between the AuNPs at higher densities [43].

An interesting observation is that the saturation in AuNP adsorption (as seen from the signs of saturation in the plasmonic peak intensities and peak shifts, Fig. 5c) to be attained at $[\text{AuNP}]_{\text{solution}}/[\text{AuNP}]_{\text{ideal}}$ ratios of ~ 2. This would indicate the surface of the MCs approach saturated coverage of AuNPs at concentration of only twice the number of surface sites. This is remarkable considering that these ratios in case of planar surfaces are typically two to three orders of magnitude higher [44,45]. This indicates high AuNP capture efficiency on the MC surface, an observation that is further supported by the visibly high speed of AuNP adsorption (Video S1, Supporting Information). A high efficiency in the AuNP binding can be related to the long and flexible DEAE polymeric chains of the MC. This behavior matches with our recent report of enhanced analyte capture by tethered receptors on planar affinity biosensors [45]. The observations are also in conformity with expectations from other literature reports that have theoretically and experimentally investigated the role of tether flexibility [46–50]. This would favor the choice of MCs that carry flexible and dynamic polymeric chains such as DEAE-Dextran, as compared to MCs with rigid surfaces.

3.3. Spectroscopic response of plasmonic microcarriers

High density and uniform coverage of AuNPs on AuNP@MCs make them particularly interesting candidates for surface-enhanced Raman spectroscopic detection of molecular analytes. The Raman spectra of the uncoated MCs matches with an earlier report in the literature for DEAE-Dextran [51]. There are no discernible differences in the spectra between the dry and wet MCs, as expected, as the swelling is not accompanied by any changes to the chemical structure or composition (Fig. S6). An additional peak at 1580 cm^{-1} that appears in the Raman spectra of AuNP@MCs (Fig. S6) can be attributed to asymmetric COO stretch of citrate ligands on the AuNPs [52]. To evaluate the sensing performance, the AuNP@MCs exhibiting saturated coverage of AuNPs (MC corresponding to C9, Fig. 5a) was functionalized with 1-naphthalene thiol (NT) chosen as a model target analyte. NT is well suited as a probe analyte given its well-defined and studied spectroscopic characteristics and ease of conformal coverage on the AuNPs. For these tests, the AuNP@MCs were incubated in an ethanolic solution of NT at a concentration of 100 µM for duration of 10 h. After incubation, the microcarriers were washed at least 5 times with absolute ethanol to

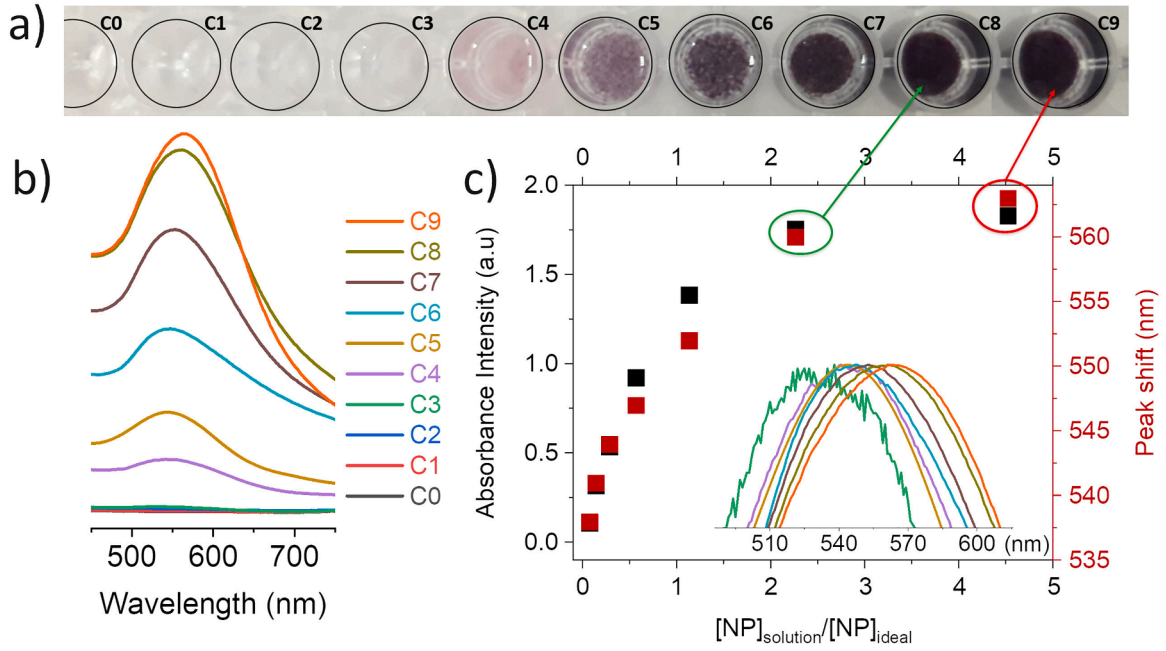

Fig. 5. Optical response of the AuNP@MCs as function of AuNP concentration. (a) Photographs of well plates with suspensions of AuNP coated microcarriers with increasing $[AuNP]_{solution}$ from C1-C9, (b) with the corresponding absorbance spectra showing a continuous increase in the intensities and the wavelength. (c) Plot showing increase in LSPR peak intensity and wavelength as a function of $[AuNP]_{solution}/[AuNP]_{ideal}$ which is the ratio of the AuNP solution concentrations in relation to the surface concentration corresponding to an ideal monolayer on a single MC.

remove unbounded and loosely bounded NT molecules before Raman measurements.

The Raman spectra of NT on AuNP@MC show clear differences in spectral intensities under dry versus wet (aqueous) state, and upon visible laser excitation at 633 nm versus 785 nm wavelengths. (Fig. 6b, c). The SERS intensity of the most intense peak at 1370 cm^{-1} corresponding to ring stretching vibration of NT was used to compare the SERS spectra. The SERS signal intensities were found to be an order of magnitude higher for the dry AuNP@MCs as compared to wet measurements (Fig. 6b,c). The AuNP@MCs is swollen under wet conditions, resulting in a greater interparticle distance between the AuNPs. However, the huge reduction in the MC volume during drying is expected to increase proximity between adjacent AuNPs, resulting in formation of intense electromagnetic (EM) hotspots and NT molecules trapped within these hotspots. Molecules present at the EM hot-spots are known to make disproportionately high signal contributions, [18–20,53] which would explain the high signal intensities observed under dry conditions. As comparison, self-assembled monolayers of NT at their saturated densities on a planar gold surface do not show any peaks in their spectra under identical conditions, indicating thus, the favorable role of interparticle EM hot-spots towards the observed spectroscopic signals in case of AuNP@MCs.

Further understanding of the structure-dependent spectroscopic properties can be drawn from the wavelength dependence of SERS intensities under wet and dry conditions. The SERS intensities of NT on AuNP@MCs in wet conditions, was found to be relatively higher for 633 nm excitation, as compared to 785 nm excitation (Fig. 6b). However, the scenario was opposite when probed under dry conditions, where the Raman intensities were higher at 785 nm as compared to 633 nm (Fig. 6c, right). The observation can be rationalized considering that a higher SERS intensity would result from the proximity of the excitation wavelength to the absorbance maxima of the AuNP@MC (Fig. 6a). However, upon drying, the formation of electromagnetic hotspots would result in strong interparticle plasmonic coupling that would lower the energy to excite the hotspots, favoring thus, the 785 nm excitation over 633 nm excitation. Several evidences in literature have pointed to how such near field effects on hotspot surfaces would often go unnoticed in the (far-field) absorbance spectra[54,55].

The different observations based on optical and spectroscopic response of AuNP@MCs in the swollen and collapsed state, align well with expectations based on the structure of the AuNP@MCs. The hydrogel behavior of the AuNP@MCs contribute in multiple ways, including enhanced trapping of AuNPs, enhanced analyte capture at inter-particle hotspots, and would prospectively also contribute to reducing non-specific binding when the AuNP@MCs are used in future as biosensors in cell-culture media.

While the prospect of using AuNP@MCs for detection/monitoring of biomarkers from cells is clearly attractive, further progress will be necessary to realize this potential- (a) surface area per microcarrier together with the large number of microcarriers in the medium could inherently limit capability for ultra-low detection limits for biomarkers in the culture medium. However, the presence of the sensor at the immediate vicinity of the biological cells can be a huge benefit to overcome diffusion limitations, and to detect/monitor biomarkers in the regions where cells are in contact with the AuNP@MCs. This will further require identifying measurement configurations that can effectively collect the spectroscopic signals of the suspended microcarrier. (b) The highest sensitivity in SERS measurements were achieved for dry AuNP@MCs, while the need for drying limits its usefulness in online measurements. This concern can be addressed by isolating, drying and investigating individual microcarriers, without impacting the large number of microcarriers still present in the cell-culture medium. This will also make it easy to subject the AuNP@MCs to end-point assays such as fluorescence immunosandwich assays. Alternatively, other approaches including metal-enhanced fluorescence as well as refractive index sensing based on LSPR shifts should be explored. Use of refractive index based sensing would provide an effective means to label-free, online measurements. The optical/spectroscopic characteristics of the AuNP@MCs can be engineered for highly sensitive LSPR or MEF based sensing, by adopting non-spherical metal nanostructures including nanorods, nanostars, or nanoshells, of gold or silver. (c) Investigations should also focus on choosing the most appropriate plasmonic sensing modality (SERS, MEF, or refractive-index sensing) in relation to the biomarkers of interest.

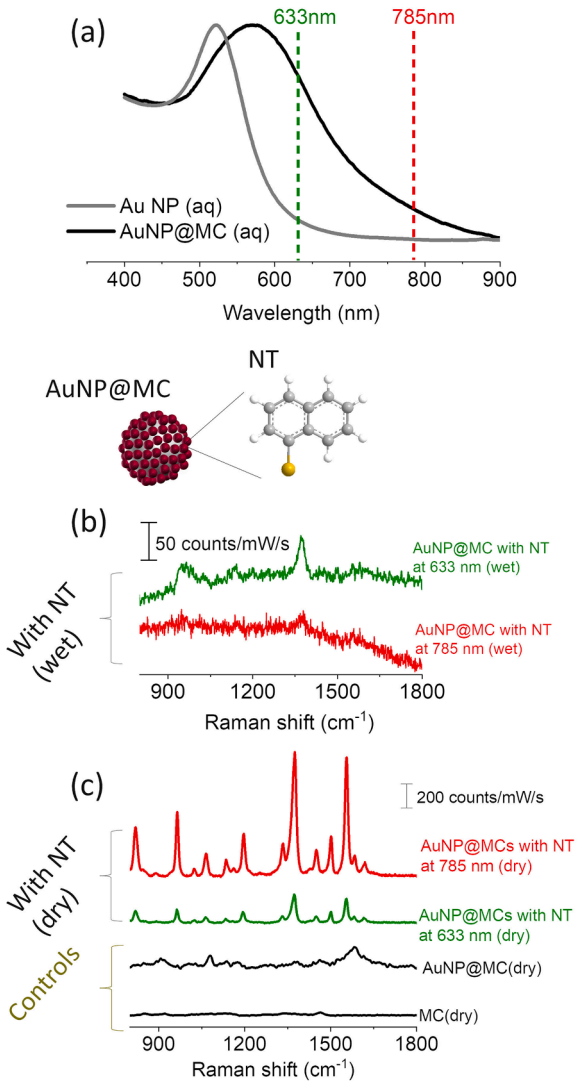

Fig. 6. SERS spectral characteristics of AuNP@MCs. (a) Comparison of the absorption spectra of AuNPs (aq) and AuNP@MCs (aq) with respect to the 633 nm and 785 nm laser excitation wavelengths used for SERS. (b,c) SERS spectra of saturated density of NT on AuNP@MCs at 633 nm and 785 nm excitation wavelengths compared under (b) wet and (c) dry conditions. (c) Raman spectra of AuNP@MCs and MCs are shown for reference.

3.4. Cell adherence, growth and migration assays on plasmonic microcarriers

AuNP@MCs were subjected to different cell biology tests to assess the impact of the AuNP coating on its cytocompatibility and performance as cell-growth support. These tests compared the growth, proliferation, and migration of human mesenchymal stem cells (hMSCs) on AuNP@MCs with uncoated counterparts. A live/dead cell assay was performed by staining with Calcein AM and Ethidium Homodimer-1 (EthD-1) to stain live (green) and dead (red) cells, respectively. The quantification of cell viability was made by fluorescence microscopy. Results show the cells to colonize AuNP@MCs to a large extent indicating their cytocompatibility. Before cell culture, MC were preserved in PBS and autoclaved at 120 °C to sterilize them [56]. Results show autoclaving to decrease the adhesion of the cells on the AuNP@MCs (Fig. 8). However, the autoclaving did not appear to affect the interaction between AuNPs and MC. The decrease in cell-adhesion on autoclaved AuNP@MCs could be a result of temperature-induced conformational changes of polymer chains in contact with the citrate-gold nanoparticles that could have resulted in changes to surface charge distribution at the interface with the cells. In future, the autoclaving step could be susbtituted by sterilizing the AuNP@MCs using ethanol. Alternatively, the AuNPs can be functionalized with cell-adhesive moieties such as RGD peptide sequences.

In the next step, the cell growth kinetics was monitored in flasks by measuring the time evolution of the concentration in glucose and lactate on a daily basis (Fig. 7). Glucose is the primary source for mammalian cells to generate energy (ATP) by oxidative phosphorylation or by anaerobic glycolysis and lactic fermentation [57]. Glucose consumption by the cells is accompanied by the production of other metabolites such as lactate and ammonia, which, at high concentrations, could inhibit cell growth. Monitoring glucose consumption and lactate production are thus important for cell growth. Results of cell growth kinetics reveal the glucose consumption by cells grown on AuNP@MCs to be similar to that on MCs (Fig. 7). The consumption rate of glucose slows down when glucose becomes limited, with the consequent decrease in production rate of lactate. Thus, there are no significant differences observed in cell growth kinetics between the MCs and AuNP@MCs.

Finally, a migration assay was performed to assess if the cells cultured on MCs could migrate to AuNP@MCs when they are introduced later to the cell culture medium. Such migration would mean that the cells do not perceive a significant difference between MC and AuNP@MC. The migration assay was performed by adding AuNP@MCs (non-autoclaved) to a medium consisting of cells cultured on MCs for a duration of 4 days. The cells were stained with DAPI and quantified on a daily basis using fluorescence microscopy (Fig. 9). Results show that the cells were able to migrate to the freshly added AuNP@MC, (Fig. 9d) confirming again the capability of the AuNP@MCs to support cell-expansion functions. Such inter-MC migration of cells, also called, 'bead-to-bead transfer' is used a key strategy to increase the available surface area during the course of cell culture [58]. This step has been shown to improve yield and performance of cell culture by avoiding the need for pre-mature harvesting of cells. The transfer between the MCs to AuNP@MCs serves as a strong indication of the similarity in cell responses between the coated and uncoated MCs.

Conclusions

Plasmonic microcarriers (AuNP@MCs) capable of molecular sensing as well as cell-expansion were demonstrated using simple and readily scalable route based on electrostatic self-assembly of AuNPs onto DEAE-

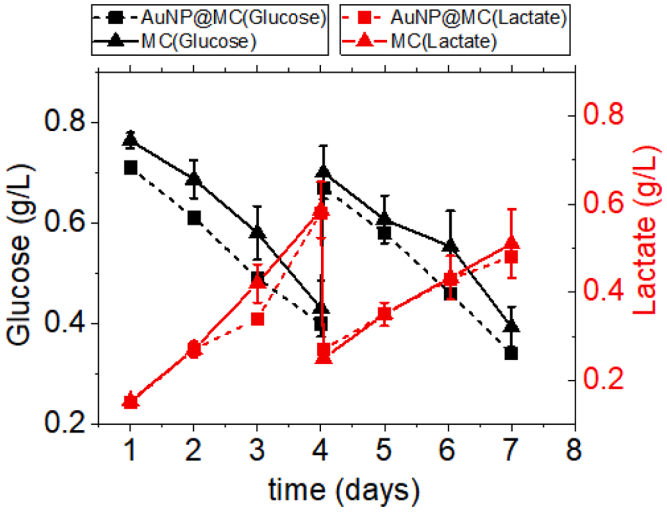

Fig. 7. Comparison of growth kinetics of hMSCs on AuNP@MCs versus MCs. Plot shows a similarity in glucose consumption (black) and lactate production (red) by cells grown on AuNP@MCs (filled squares, dotted lines) and MCs (filled triangles, solid lines).

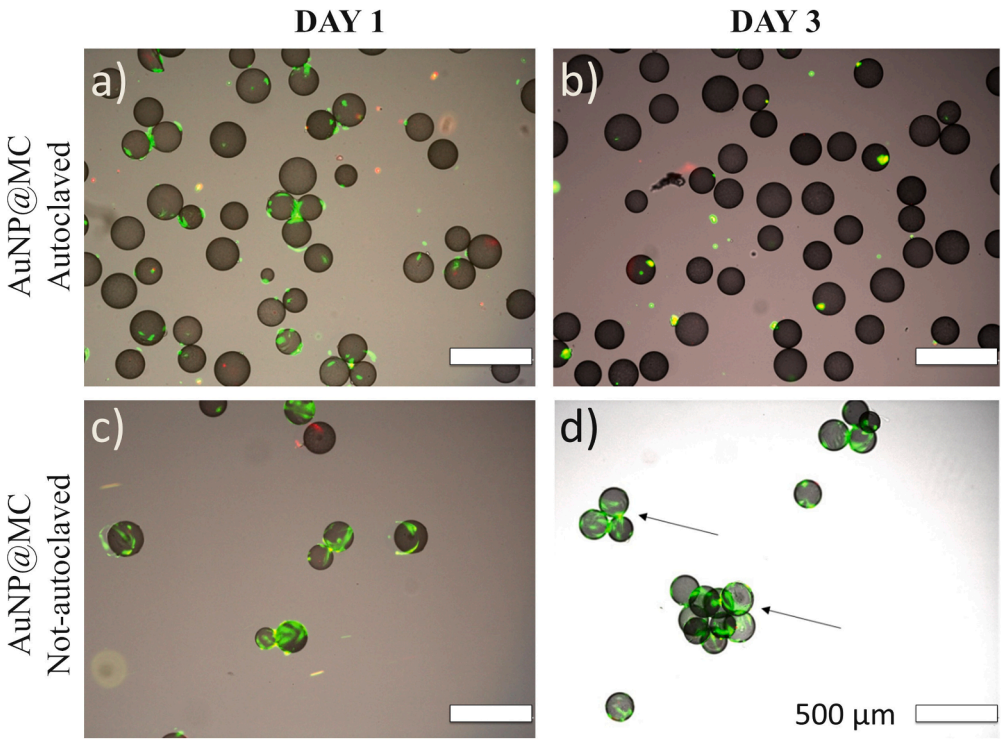

Fig. 8. Comparison of the influence of autoclaving. Fluorescence microscopy images showing (a,b) reduced cell growth on AuNP@MCs when autoclaved, as compared to (c,d) AuNP@MCs without autoclaving. For both cases, cell culture results are shown after 1 day (a,c) and 3 days (b,d).

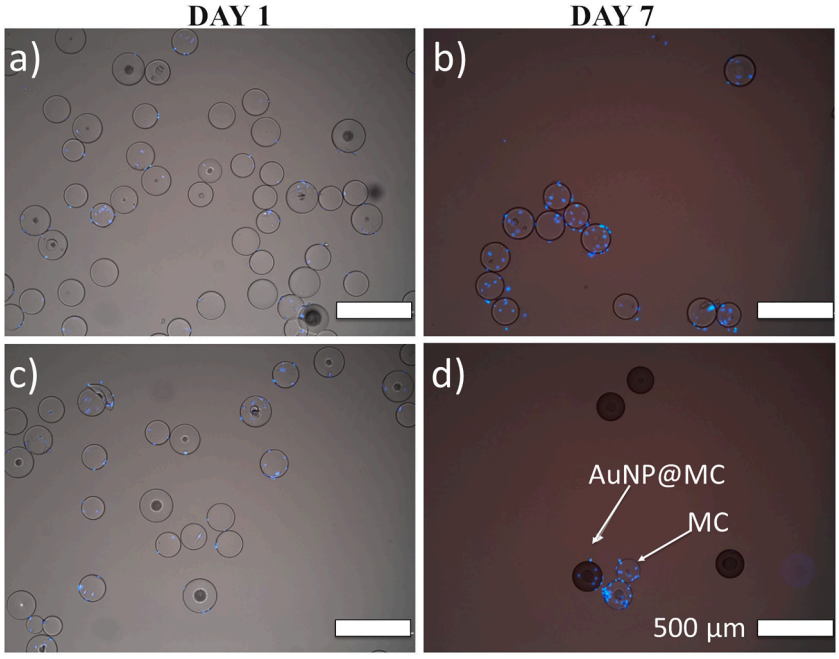

Fig. 9. Bead-to-Bead migration of hMSC between MCs and AuNP@MCs. (a-d) Fluorescence microscopy images of hMSCs on (a) MCs after 1 day (b) and 7 days, (c) MCs after 1 day and (d) MCs & AuNP@MCs after 7 days of culture (AuNP@MCs were added after 4 days of hMSC culture on MCs).

Dextran microcarriers (MCs). Detailed understanding of the internal and external structure of the AuNP@MC through a combination of optical microscopy, SEM, AFM, ultramicrotomy, and nano-SIMS permitted the ease of geometric modeling to deduce the structure and distribution of AuNP assemblies. The successful formulation of geometric models opens opportunities to rationally design AuNP@MCs and to understand / predict outcomes of the optical/spectroscopic response as well as cell-growth outcomes. The hydrogel characteristics of the DEAE-Dextran was found to profoundly enhance the density and kinetics of AuNP binding. The swelling and collapse of the AuNP@MCs provides unique possibilities to realize high density of inter-particle electromagnetic hotspots and analyte trapping at the hot-spots, favoring high sensitivity in molecular sensing. AuNP@MCs were found to retain cell expansion functions including growth kinetics, viability and inter-MC migration of

human mesenchymal stem cells.

Future work is necessary to ascertain the purity of cells to rule out potential long-term effects, and to demonstrate assays to detect or quantify proteins and other biomarkers secreted by the cells attached to the AuNP@MC surface. The AuNP@MCs carry the potential to be turned into in-vitro models where the embedded plasmonic sensing functions can play a unique role in monitoring the behavior of attached cells. Spherical AuNPs can be substituted by other plasmonic nanostructures with non-spherical morphologies, including nanostars, nanoshells, or nanorods, to enable multimodal and highly sensitive biomarker detection by following refractive index-dependent LSPR shifts, together with surface-enhanced Raman and fluorescence detection. Another interesting direction is to investigate the ability to release cells from the surface of AuNP@MCs by leveraging plasmonic heating effects. The present study serves as a key step forward towards design and engineering of new types of suspended 3D plasmonic cell-growth structures that can be leveraged for multiple sectors including, cell-expansion, in-vitro models, tissue-engineering scaffolds and in-vitro diagnostics.

Authors' contribution

C.B.A. Stoffels, P. Grysan, R. Rastogi, M. Beggiato, S. Krishnamoorthy contributed to Investigations, Methodology, Validation related to fabrication and characterization of MCs and AuNP@MCs. C. Sion, E. Olmos contributed to Methodology, Investigation and Validation related to cell-biology experiments. E. Olmos contributed to Supervision, Funding acquisition & Project administration (IMPROVE-STEM). S. Krishnamoorthy contributed to Conceptualization, Supervision, Funding acquisition & Project administration for PLASENS, MASSENA, and IMPROVE-STEM (with EO). All authors contributed to Writing, Review, Editing and Visualization.

Declaration of Competing Interest

The authors declare that they have no known competing financial interests or personal relationships that could have appeared to influence the work reported in this paper.

Data availability

Data will be made available on request.

Acknowledgments

Authors thank Esther Lentzen for NanoSIMS measurements and Asmaa El Moul for Ultramicrotomy. Funding from INTERREG Grand Region V via IMPROVE-STEM project, and Fonds National de la Recherche (FNR) Luxembourg via MASSENA and PLASENS (C15/MS/10459961) projects is gratefully acknowledged.

Supplementary materials

Supplementary material associated with this article can be found, in the online version, at doi:10.1016/j.snr.2023.100173.

References

[1] A.F. Coskun, A.E. Cetin, B.C. Galarreta, D.A. Alvarez, H. Altug, A. Ozcan, Lensfree optofluidic plasmonic sensor for real-time and label-free monitoring of molecular binding events over a wide field-of-view, Sci. Rep. 4 (2014) 1–7, https://doi.org/10.1038/srep06789.

[2] O.I. Guliy, B.D. Zaitsev, S.K. Mehta, I.A. Borodina, Analysis of microbial cell viability in a liquid using an acoustic sensor, Ultrasound Med. Biol. 46 (2020) 1026–1039, https://doi.org/10.1016/j.ultrasmedbio.2019.12.010.

[3] M.M. Bilek, D.R. McKenzie, Plasma modified surfaces for covalent immobilization of functional biomolecules in the absence of chemical linkers: towards better biosensors and a new generation of medical implants, Biophys. Rev. 2 (2010) 55–65, https://doi.org/10.1007/s12551-010-0028-1.

[4] A. Weltin, K. Slotwinski, J. Kieninger, I. Moser, G. Jobst, M. Wego, R. Ehret, G. A. Urban, Cell culture monitoring for drug screening and cancer research: a transparent, microfluidic, multi-sensor microsystem, Lab Chip 14 (2014) 138–146, https://doi.org/10.1039/c3lc50759a.

[5] J. Sabaté del Río, J. Ro, H. Yoon, T.-E. Park, Y.-K. Cho, Integrated technologies for continuous monitoring of organs-on-chips: current challenges and potential solutions, Biosens. Bioelectron. 224 (2023), 115057, https://doi.org/10.1016/j.bios.2022.115057.

[6] S. Fuchs, S. Johansson, A.Ø. Tjell, G. Werr, T. Mayr, M. Tenje, In-line analysis of organ-on-chip systems with sensors: integration, fabrication, challenges, and potential, ACS Biomater. Sci. Eng. 7 (2021) 2926–2948.

[7] P.S. Couto, M.C. Rotondi, A. Bersenev, C.J. Hewitt, A.W. Nienow, F. Verter, Q. A. Rafiq, Expansion of human mesenchymal stem/stromal cells (hMSCs) in bioreactors using microcarriers: lessons learnt and what the future holds, Biotechnol. Adv. (2020), 107636.

[8] A. Ornelas-González, M. González-González, M. Rito-Palomares, Microcarrier-based stem cell bioprocessing: GMP-grade culture challenges and future trends for regenerative medicine, Crit. Rev. Biotechnol. (2021) 1–15.

[9] B. Koh, N. Sulaiman, M.B. Fauzi, J.X. Law, M.H. Ng, R.B.H. Idrus, M.D. Yazid, Three dimensional microcarrier system in mesenchymal stem cell culture: a systematic review, Cell Biosci 10 (2020) 1–16.

[10] X. Li, M. Soler, C. Szydzik, K. Khoshmanesh, J. Schmidt, G. Coukos, A. Mitchell, H. Altug, Label-free optofluidic nanobiosensor enables real-time analysis of single-cell cytokine secretion, Small 14 (2018) 1–11, https://doi.org/10.1002/smll.201800698.

[11] Q. Han, E.M. Bradshaw, B. Orn Nilsson, D.A. Hafler Cd, J.C. Love, Multidimensional analysis of the frequencies and rates of cytokine secretion from single cells by quantitative microengraving †, Lab. Chip. 10 (2010) 1337–1492, https://doi.org/10.1039/b926849a.

[12] A.J. Torres, A.S. Hill, J.C. Love, Nanowell-based immunoassays for measuring single-cell secretion: characterization of transport and surface binding, Anal. Chem. 86 (2014) 34, https://doi.org/10.1021/ac4030297.

[13] A.T. Young, K.R. Rivera, P.D. Erb, M.A. Daniele, Monitoring of microphysiological systems: integrating sensors and real-time data analysis toward autonomous decision-making, ACS Sens. 4 (2019) 1454–1464, https://doi.org/10.1021/acssensors.8b01549.

[14] C. Ma, R. Fan, H. Ahmad, Q. Shi, B. Comin-Anduix, T. Chodon, R.C. Koya, C.C. Liu, G.A. Kwong, C.G. Radu, A. Ribas, J.R. Heath, A clinical microchip for evaluation of single immune cells reveals high functional heterogeneity in phenotypically similar T cells, Nat. Med. 17 (2011) 738–743, https://doi.org/10.1038/nm.2375.

[15] K. Braeckmans, S.C. De Smedt, M. Leblans, R. Pauwels, J. Demeester, Encoding microcarriers: present and future technologies, Nat. Rev. Drug Discov. 1 (2002) 447–456.

[16] V.A. Sabetsky, S.V. Martiouchine, Z.V. Nesterova, Development of novel optically encoded microspheres for microarrays, in: Proceeding of the SPIE - International Soc. Opt. Eng., Inst. of Highly Pure Biopreparations, 7 Pudozhskaya str, St. Petersburg, Russian Federation, 2002, pp. 78–81, 197110.

[17] A. Vafajoo, A. Rostami, S.F. Parsa, R. Salarian, N. Rabiee, G. Rabiee, M. Rabiee, M. Tahriri, D. Vashaee, L. Tayebi, Multiplexed microarrays based on optically encoded microbeads, Biomed. Microdevices. 20 (2018) 1–14.

[18] R. Rastogi, H. Arianfard, D. Moss, S. Juodkazis, P.-M. Adam, S. Krishnamoorthy, Analyte Co-localization at electromagnetic gap hot-spots for highly sensitive (bio) molecular detection by plasmon enhanced spectroscopies, ACS Appl. Mater. Interfaces. 13 (2021) 9113–9121, https://doi.org/10.1021/acsami.0c17929.

[19] R. Rastogi, E.A. Dogbe Foli, R. Vincent, S. Poovathingal, P.-M. Adam, S. Krishnamoorthy, Hierarchically structured plasmonic nanoparticle assemblies with dual-length scale electromagnetic hot spots for enhanced sensitivity in the detection of (bio)molecular analytes, J. Phys. Chem. C. 125 (2021) 8647–8655, https://doi.org/10.1021/acs.jpcc.0c10467.

[20] Y. Fang, N.H. Seong, D.D. Dlott, Measurement of the distribution of site enhancements in surface-enhanced raman scattering, Science 321 (80) (2008) 388–392, https://doi.org/10.1126/science.1159499.

[21] N. Ferreyra, L. Coche-Guérente, J. Fatisson, M. Lopez Teijelo, P. Labbé, Layer-by-layer self-assembled multilayers of redox polyelectrolytes and gold nanoparticles, Chem. Commun. 3 (2003) 2056–2057, https://doi.org/10.1039/b305347d.

[22] H. Malekzad, M. Beggiato, D. Hegemann, S. Gaiser, D. Duday, S. Krishnamoorthy, Rational route to fabrication of uni-dimensional surface gradients presenting stochastic and periodic arrangement of nanoparticles, Appl. Surf. Sci. 581 (2022), 151763, https://doi.org/10.1016/j.apsusc.2021.151763.

[23] E.M.S. Azzam, A. Bashir, O. Shekhah, A.R.E. Alawady, A. Birkner, C. Grunwald, C. Wöll, Fabrication of a surface plasmon resonance biosensor based on gold nanoparticles chemisorbed onto a 1,10-decanedithiol self-assembled monolayer, Thin Solid Films 518 (2009) 387–391, https://doi.org/10.1016/J.TSF.2009.07.120.

[24] S.R. Ahmed, J. Kim, V.T. Tran, T. Suzuki, S. Neethirajan, J. Lee, E.Y. Park, In situ self-assembly of gold nanoparticles on hydrophilic and hydrophobic substrates for influenza virus-sensing platform, Sci. Rep. 7 (2017) 44495, https://doi.org/10.1038/srep44495.

[25] S. Krishnamoorthy, S. Krishnan, P. Thoniyot, H.Y. Low, Inherently reproducible fabrication of plasmonic nanoparticle arrays for SERS by combining nanoimprint and copolymer lithography, ACS Appl. Mater. Interfaces. 3 (2011), https://doi.org/10.1021/am1011518.

[26] S. Maenosono, T. Okubo, Y. Yamaguchi, Overview of nanoparticle array formation by wet coating, J. Nanoparticle Res. 5 (2003) 5–15.

[27] S. Namsani, J.K. Singh, Dewetting dynamics of a gold film on graphene: implications for nanoparticle formation, Faraday Discuss 186 (2016) 153–170, https://doi.org/10.1039/C5FD00118H.
[28] E.L. Hinrichsen, J. Feder, T. Jøssang, Geometry of random sequential adsorption, J. Stat. Phys. 44 (1986) 793–827, https://doi.org/10.1007/BF01011908.
[29] T. Zhu, X. Fu, T. Mu, J. Wang, Z. Liu, pH-dependent adsorption of gold nanoparticles on p-aminothiophenol-modified gold substrates, Langmuir 15 (1999) 5197–5199, https://doi.org/10.1021/la990081g.
[30] K. Kim, H. Ryoo, Y.M. Lee, K.S. Shin, Adsorption characteristics of Au nanoparticles onto poly(4-vinylpyridine) surface revealed by QCM, AFM, UV/vis, and Raman scattering spectroscopy, J. Colloid Interface Sci. 342 (2010) 479–484, https://doi.org/10.1016/j.jcis.2009.10.019.
[31] A. Reznickova, Z. Kolska, J. Siegel, V. Svorcik, Grafting of gold nanoparticles and nanorods on plasma-treated polymers by thiols, J. Mater. Sci. 47 (2012) 6297–6304, https://doi.org/10.1007/s10853-012-6550-8.
[32] W. Zhao, X. Liu, Y. Xu, S. Wang, T. Sun, S. Liu, X. Wu, Z. Xu, Polymer nanopillar array with Au nanoparticle inlays as a flexible and transparent SERS substrate, RSC Adv 6 (2016) 35527–35531, https://doi.org/10.1039/C6RA06329B.
[33] J. Cheng, Y. Liu, H. Mao, W. Zhao, Y. Ye, Y. Zhao, L. Zhang, M. Li, C. Huang, Wafer-level fabrication of 3D nanoparticles assembled nanopillars and click chemistry modification for sensitive SERS detection of trace carbonyl compounds, Nanotechnology 31 (2020), 265301.
[34] F.L. Yap, P. Thoniyot, S. Krishnan, S. Krishnamoorthy, Nanoparticle cluster arrays for high-performance sers through directed self-assembly on flat substrates and on optical fibers, ACS Nano 6 (2012) 2056–2070, https://doi.org/10.1021/nn203661n.
[35] C. Paquet, H.W. de Haan, D.M. Leek, H.-Y. Lin, B. Xiang, G. Tian, A. Kell, B. Simard, Clusters of superparamagnetic iron oxide nanoparticles encapsulated in a hydrogel: a particle architecture generating a synergistic enhancement of the T2 relaxation, ACS Nano 5 (2011) 3104–3112, https://doi.org/10.1021/nn2002272.
[36] D. Xu, H. Lv, B. Liu, Encapsulation of metal nanoparticle catalysts within mesoporous zeolites and their enhanced catalytic performances: a review, Front. Chem. 6 (2018) 550.
[37] M. Chirea, V. García-Morales, J.A. Manzanares, C. Pereira, R. Gulaboski, F. Silva, Electrochemical characterization of polyelectrolyte/gold nanoparticle multilayers self-assembled on gold electrodes, J. Phys. Chem. B. 109 (2005) 21808–21817, https://doi.org/10.1021/jp0537815.
[38] S. Mühlig, D. Cialla, A. Cunningham, A. März, K. Weber, T. Bürgi, F. Lederer, C. Rockstuhl, Stacked and tunable large-scale plasmonic nanoparticle arrays for surface-enhanced raman spectroscopy, J. Phys. Chem. C. 118 (2014) 10230–10237, https://doi.org/10.1021/jp409688p.
[39] J. Turkevich, Colloidal gold. Part II, Gold Bull. 18 (1985) 125–131, https://doi.org/10.1007/bf03214694.
[40] J. Turkevich, P.C. Stevenson, J. Hillier, A study of the nucleation and growth processes in the synthesis of colloidal gold, Discuss. Faraday Soc. 11 (1951) 55–75.
[41] J. Turkevich, Colloidal gold. Part I - Historical and preparative aspects, morphology and structure, Gold Bull 18 (1985) 86–91, https://doi.org/10.1007/BF03214690.
[42] K. Nilsson, Microcarrier cell culture, Biotechnol. Genet. Eng. Rev. 6 (1988) 403–439, https://doi.org/10.1080/02648725.1988.10647854.
[43] T.A. Kolesnikova, D. Kohler, A.G. Skirtach, H. Möhwald, Laser-induced cell detachment, patterning, and regrowth on gold nanoparticle functionalized surfaces, ACS Nano 6 (2012) 9585–9595, https://doi.org/10.1021/nn302891u.
[44] M. Beggiato, R. Rastogi, C. Dupont-Gillain, S. Krishnamoorthy, Confined adsorption within nanopatterns as generic means to drive high adsorption efficiencies on affinity sensors, Sens. Actuat. B Chem. 366 (2022), 131945, https://doi.org/10.1016/j.snb.2022.131945.
[45] M. Beggiato, H. Payen, C. Dupont-Gillain, S. Krishnamoorthy, Impact of tether length and flexibility on the efficiency of analyte capture by tethered receptors, Sens. Actuat. Rep. 5 (2023), 100148, https://doi.org/10.1016/j.snr.2023.100148.
[46] N.W. Moore, T.L. Kuhl, The role of flexible tethers in multiple ligand-receptor bond formation between curved surfaces, Biophys. J. 91 (2006) 1675–1687, https://doi.org/10.1529/biophysj.105.079871.
[47] M. Maaloum, A. Courvoisier, Elasticity of single polymer chains, Macromolecules 32 (1999) 4989–4992, https://doi.org/10.1021/ma981023p.
[48] C. Jeppesen, Impact of polymer tether length on multiple ligand-receptor bond formation, Science 293 (80) (2001) 465–468, https://doi.org/10.1126/science.293.5529.465.
[49] A.G. Moreira, C.M. Marques, The role of polymer spacers in specific adhesion, J. Chem. Phys. 120 (2004) 6229–6237, https://doi.org/10.1063/1.1651088.
[50] D. Reeves, K. Cheveralls, J. Kondev, Regulation of biochemical reaction rates by flexible tethers, Phys. Rev. E. 84 (2011) 21914, https://doi.org/10.1103/PhysRevE.84.021914.
[51] L. Mikac, T. Jurkin, G. Štefanić, M. Ivanda, M. Gotić, Synthesis of silver nanoparticles in the presence of diethylaminoethyl-dextran hydrochloride polymer and their SERS activity, J. Nanoparticle Res. 19 (2017) 1–12, https://doi.org/10.1007/s11051-017-3989-1.
[52] M.A. Verschuuren, M. Megens, Y. Ni, H. van Sprang, A. Polman, Large area nanoimprint by substrate conformal imprint lithography (SCIL), Adv. Opt. Techn. 6 (2017) 243–264, https://doi.org/10.1515/aot-2017-0022.
[53] R. Rastogi, E.A. Dogbe Foli, R. Vincent, P.-M. Adam, S. Krishnamoorthy, Engineering electromagnetic hot-spots in nanoparticle cluster arrays on reflective substrates for highly sensitive detection of (bio)molecular analytes, ACS Appl. Mater. Interfaces. 13 (2021) 32653–32661, https://doi.org/10.1021/acsami.1c01953.
[54] S.L. Kleinman, B. Sharma, M.G. Blaber, A.-I. Henry, N. Valley, R.G. Freeman, M. J. Natan, G.C. Schatz, R.P. Van Duyne, Structure enhancement factor relationships in single gold nanoantennas by surface-enhanced Raman excitation spectroscopy, J. Am. Chem. Soc. 135 (2013) 301–308.
[55] M.G. Blaber, G.C. Schatz, Extending SERS into the infrared with gold nanosphere dimers, Chem. Commun. 47 (2011) 3769–3771.
[56] *Cytodex® 1 Microcarrier Beads*, Sigma-Aldrich. (n.d.).
[57] D. Schop, F.W. Janssen, L.D.S. van Rijn, H. Fernandes, R.M. Bloem, J.D. de Bruijn, R. van Dijkhuizen-Radersma, Growth, metabolism, and growth inhibitors of mesenchymal stem cells, Tissue Eng. Part A. 15 (2009) 1877–1886.
[58] Q.A. Rafiq, S. Ruck, M.P. Hanga, T.R.J. Heathman, K. Coopman, A.W. Nienow, D. J. Williams, C.J. Hewitt, Qualitative and quantitative demonstration of bead-to-bead transfer with bone marrow-derived human mesenchymal stem cells on microcarriers: utilising the phenomenon to improve culture performance, Biochem. Eng. J. 135 (2018) 11–21.

Charlotte Stoffels obtained her master's in chemical and materials engineering from the University of Liège in 2018, with an internship in the Nano-Enabled Medicine and Cosmetics (NEMC) group of LIST and her master's in biomedical engineering from the University of Liège in 2019, with an internship in the Environmental Health (EH) group of LIST. She is currently a PhD candidate in the Advanced Instrumentation for Nano-Analytics (AINA) group of LIST and at the University of Luxembourg. She is working on the development of a new methodology using high-resolution chemical imaging techniques allowing the localization of PFAS, inside cells and tissues.

Patrick Grysan is a Research Engineer at Luxembourg Institute of Science and Technology (LIST). He received his Engineering degree from Ecole Nationale de Chimie de Mulhouse in 2005. After a short experience at Arkema centre de Recherche de l'Est on analysis of Acrylates he joined LIST to focus on surface characterization, first with Secondary Ions Mass Spectroscopy (NanoSIMS50) and since 8 years dealing with the Local Probes diversity of analytical solutions.

Caroline Sion obtained her PhD working at the LRGP team of University of Lorraine, and is currently an engineer at StemInov, working on the optimization of the process of mesenchymal stem cells production in bioreactors. She holds an engineering diploma in Agronomy and Biotechnology from ENSAIA, a masters degree in business administration and has worked as R&D intern in Agriculture and Agri-Food Canada, Poietis, France, and CNRS.

Rishabh Rastogi completed his Masters from Amity University in India in 2015 and his PhD degree from the University Technology of Troyes in France and LIST in 2020. His-PhD thesis focused on engineering electromagnetic hotspots for highly sensitive biomolecular detection by plasmon-enhanced spectroscopies. He is currently a member of staff of ASM, Belgium.

Matteo Beggiato completed his Masters from Politecnico di Torino in Italy in 2017 and obtained his PhD degree from the University of Luxembourg, and LIST in 2021. His-PhD thesis focused on investigating Nanoengineered Interfaces to Enhance Analyte Mass Transport and Analyte Capture - Towards High Performance Affinity Biosensors. He is now a member of staff of IMEC, Belgium.

Eric Olmos is a professor of biotechnological process engineering at ENSAIA Nancy (University of Lorraine). with research activities around the intensification, optimization and extrapolation of animal (CHO, VERO), human (CSM of Wharton jelly) or bacterial cell culture processes. For this, strategies coupling implementation of cultures in agitated bioreactors, online monitoring of culture parameters, kinetic modeling and CFD simulation of flows are developed. He is responsible for the Master in Industrial Biotechnology (BioIN) and teaching units dedicated to the design and extrapolation of animal and human cell culture bioreactors.

Sivashankar Krishnamoorthy received his PhD degree from CSEM SA, Neuchatel, and EPFL, Switzerland, in 2006. He has over 18 years of experience in the research and development of advanced nanotechnologies in micro/nanofabrication, bio-interfaces, nanooptics and functional integration of engineered nanostructures within optical and electronic devices. He currently leads the projects focused on nanoengineered biological devices and biointerfaces at the Luxembourg Institute of Science and Technology (LIST).